Eur. J. Mech., B/Fluids, **17,** n° 2, 239-254, 1998

Effect of a rotating magnetic field of arbitrary frequency on a liquid metal column

L. MARTIN WITKOWSKI and P. MARTY *

ABSTRACT. – We consider the influence of a rotating magnetic field on an infinitely long cylindrical liquid metal column. A solution for the flow field and magnetic field distribution is obtained for any value of the Hartmann number, Ha, and of the shielding parameter, R_ω. When $Ha \gg 1$, it has been shown that, as long as $R_\omega < \frac{Ha}{\sqrt{2}}$, the flow consists of a core rotating with the same angular velocity as that of the magnetic field and of a Hartmann boundary layer at the wall. The flow also contains recirculating eddies which are aligned with the magnetic field in the cylinder core. It is noted that the magnetic field is swept by the convective effect of the flow in the wall boundary layer whereas it satisfies a pure diffusion regime in the core. A simplified ring model permits a simple explanation of the critical value $R_\omega = \frac{Ha}{\sqrt{2}}$. © Elsevier, Paris.

1. Introduction

There are many situations in which a rotating magnetic field is a useful way to create or to control the flow of liquid metal. In metallurgy, for example, this technique has been widely used even on large scales for mixing different types of constituents or in order to remove impurities by creating a pressure gradient using the effects of centrifugal forces (Davidson and Hunt, 1987). More recently, in various technologies involving liquid metal processing, the use of a rotating magnetic field has been investigated due to its promising future as a contactless tool aiming at controlling flows (*see* Gelfgat and Priede, 1995, for a complete review).

Most of the studies have dealt with the case of an infinitely long circular cylinder filled with a liquid metal and located in the gap of a stator composed of primary alternating currents which create the rotating field (Moffatt, 1978). In some particular cases, due to the simplicity of this geometry, analytical solutions can be obtained. The most important results which have been already obtained will be discussed below and are summarized in figure 1. The case of a cylinder having a finite height has also been considered in the low frequency limit (Gelfgat *et al.*, 1991). In this case, the magnetic field distribution is decoupled from the momentum equations, thereby facilitating calculation of the magnetic field distribution which is the same as it would be in an insulating medium. Then a finite volume technique is used for determining the complete flow pattern.

Moffatt (1965) proposed a solution for an infinitely long cylinder restricted to the case in which the angular velocity of the liquid metal column is low in comparison to that of the magnetic field. In this paper, this situation will be referred to as the "rigid body approximation". This means that the fluid can be considered at rest with respect to the magnetic field. Moreover, in the Moffatt paper, the magnetic field frequency was assumed sufficiently high to make the ratio of the diffusion time to the electric period large compared to unity [1]. It is known that under these circumstances the fluid produces a shielding effect which confines the magnetic field into

* Laboratoire des Ecoulements Géophysiques et Industriels IMG(CNRS-UJF-INPG) BP53X – 38041 Grenoble cedex – France. e-mail: Philippe.Marty@hmg.inpg.fr

[1] This ratio, known as the shielding parameter R_ω will be defined in the following section.

0997-7546/98/02/© Elsevier, Paris

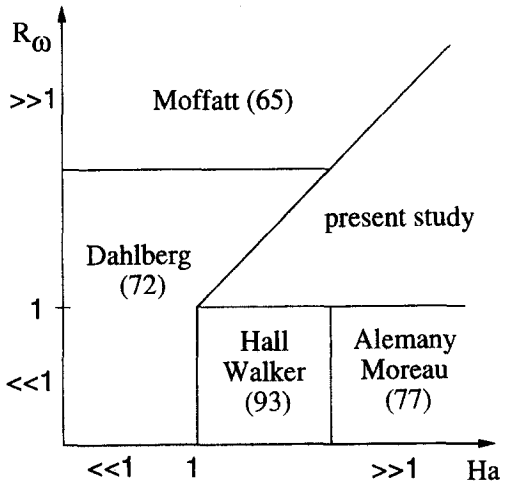

Fig. 1. – Validity map of the previous studies versus Ha and R_ω.

a thin layer at the rim of the cylinder. These two hypotheses allowed Moffatt to separate the problem into two distinct steps. The first is the resolution of the induction equation which gives the magnetic field distribution in terms of Bessel functions, together with the electric current and electromagnetic forces (some mistakes occurred in Moffatt (1965) but a corrigendum was published in 1973 (J. Fluid. Mech., vol. 58, p. 823)). It is found that the electromagnetic forces have a steady and a periodic ingredient, but only the steady part of the azimuthal component is rotational. This means that the periodic part of the force will be compensated by a pressure gradient and will not affect the mean velocity field. In a second step, Moffatt solved the Navier-Stokes equations to obtain the azimuthal velocity of this flow where the inertia forces disappear and where the electromagnetic forces are only balanced by viscous shear. The ratio of these two terms is the Hartmann number which is assumed small enough to satisfy the "rigid body approximation".

Dahlberg (1972) obtained the velocity field in terms of a series expansion for any value of R_ω. In this study too, the velocity of the fluid was assumed small in comparison with that of the magnetic field. Consequently, as in the Moffatt paper, this limits the validity of the study to situations in which the Hartmann number is small enough to neglect the influence of the azimuthal velocity of the fluid on the magnetic field distribution.

Again for an infinitely long cylinder, the case of high Hartmann numbers was considered by Alemany and Moreau (1977) in the low frequency limit ($R_\omega \ll 1$). In this study, the magnetic interaction parameter, which is the ratio of the electromagnetic forces to inertia is assumed much larger than unity. Here also, the magnetic field distribution is calculated at an early stage. Nevertheless, due to the high value of the Hartmann number, this inertialess problem has the peculiarity of presenting a coupling between the Ohm law and the Navier-Stokes equations. Moreover, the fluctuating part of the electromagnetic forces produces non-circular streamlines.

This latter study was extended by Hall and Walker (1993) who used spectral methods for solving the momentum equations. No restrictions concerning the Hartmann number were introduced in this paper and inertia is assumed negligible. As in the Alemany and Moreau (1977) study, the rotating frequency was assumed small enough to ignore any screening effect from the cylindrical column.

The bibliography reveals a lack of studies dealing with any value of the shielding parameter R_ω and of the Hartmann number Ha. This is probably due to the strong coupling which exists in this case between the electromagnetic and the dynamic equations, especially when high values are used for both R_ω and Ha. Situations in which a strong coupling between velocity and electromagnetic fields have been of interest to the MHD community for a long time. To our knowledge no papers are concerned with this problem for the case

of rotating magnetic fields. The aim of this paper is to consider the case of an infinitely long circular cylinder located inside a magnetic field rotating around its symmetry axis in just such a situation. Although not currently applicable to a practical situation, we hope it is a first step to a better physical understanding of the full coupled problem. As in Hall and Walker (1993), inertia will be neglected. The second section of this paper will present the model taken as our mathematical basis and from which a solution will be obtained. The symmetry and the dimensionless form permit the quantity of unknowns and physical parameters to be greatly reduced. Using a vector potential for the magnetic field and a stream function for the velocity field restricts the problem to a set of two partial differential equations. The numerical resolution of the set of equations allowed us to study the effect of the shielding parameter R_ω and of the Hartmann number on the flow and magnetic field solutions. The results are presented in the third section. Analysis of the results lead to a simplified model for the flow and the magnetic field. This allows the proposal of a better understanding of the essential physical mechanisms.

2. Mathematical model

2.1. Equations and boundary conditions

Consider an isothermal, incompressible, viscous fluid, contained in an electrically insulating circular tube and submitted to the magnetic field created by a surface current sheet located on the cylinder surface at $r = a$:

$$\vec{j} = -j_o \cos(p\theta - \omega t) \cdot \vec{k} \tag{1}$$

where j_o is the current density per unit length, $2p$ is the number of poles of the field and ω stands for the electric pulsation. The region outside $r = a$ is filled with material of high permeability so that we may assume $\mu = \infty$ for $r > a$. As shown in figure 2, we use the cylindrical coordinates (r, θ, z) with the unit vector $\vec{k}$ along the cylinder's vertical axis. For $r < a$, the equation for the magnetic field $\vec{B}$ is given by:

$$\frac{\partial \vec{B}}{\partial t} = \overrightarrow{\text{curl}}(\vec{V} \wedge \vec{B}) + \frac{1}{\mu\sigma} \cdot \Delta \vec{B} \tag{2}$$

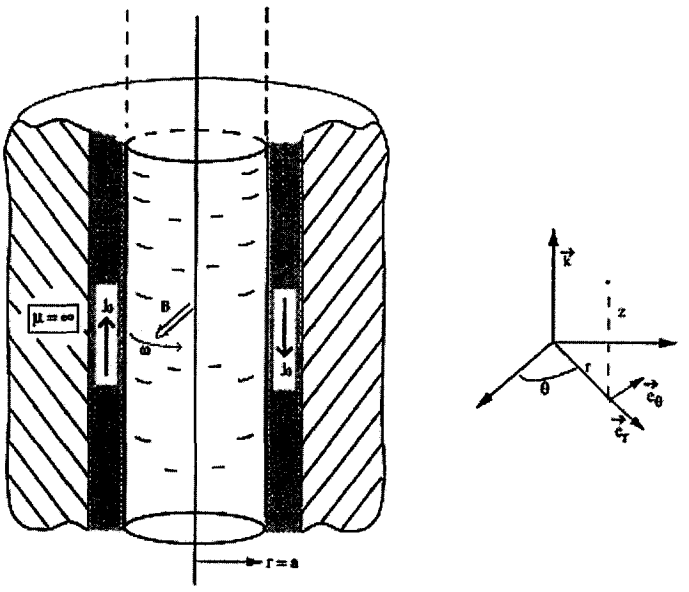

Fig. 2. – Coordinate system.

where σ and μ are the electrical conductivity and the magnetic permeability of the fluid respectively. The liquid metal motion which is created by the Lorentz forces generated by the surface current sheet is described by:

$$\mathrm{div}\vec{V} = 0 \tag{3}$$

$$\rho\left(\frac{\partial\vec{V}}{\partial t} + \vec{V}\cdot\overrightarrow{\mathrm{grad}\vec{V}}\right) = -\overrightarrow{\mathrm{grad}p} + \rho\nu\Delta\vec{V} + \vec{j}\wedge\vec{B} \tag{4}$$

where $\vec{V}$ and p are the velocity and pressure fields and where ν and ρ are the kinematic viscosity and the density of the fluid. The current density $\vec{j}$ and the electric field $\vec{E}$ are obtained using the Ohm law:

$$\vec{j} = \sigma(\vec{E} + \vec{V}\wedge\vec{B}). \tag{5}$$

The boundary conditions for the velocity field should satisfy the no-slip condition at the wall where $r = a$:

$$\vec{V} = \vec{0} \text{ for } r = a \tag{6}$$

whereas those for the magnetic field should express the continuity of the radial component in $r = a$:

$$[B_r]_{r=a} = 0 \tag{7}$$

and the jump in azimuthal component imposed by the current sheet, which can be written (Durand, 1968):

$$\left[\frac{B_\theta}{\mu}\right]_{r=a} = -j_0\cos(p\theta - \omega t). \tag{8}$$

2.2. Symmetry properties (*see* Dahlberg, 1972)

For given values of t, r, θ, a vector $\vec{a}$ will be defined as being:

$$\begin{cases}\text{even in } z \text{ if } \vec{a}(-z) = (a_r(z), a_\theta(z), -a_z(z))\\ \text{odd in } z \text{ if } \vec{a}(-z) = (-a_r(z), -a_\theta(z), a_z(z))\end{cases}$$

If $\vec{V}$, p and $\vec{B}$ are even then $\vec{E}$, $\vec{j}$ are odd. The only non-homogeneous boundary condition being an even condition for $\vec{B}$, we can conclude that $B_z = V_z = E_{r,\theta} = j_{r,\theta} = \varphi = 0$ for $z = 0$, (φ is the electrical potential). For our z-independent case ($\frac{\partial}{\partial z} = 0$), the relation must hold for all z.

2.3. Non-dimensional numbers and characteristics scales

A dimensional analysis shows that three arbitrary non-dimensional numbers can be formed. The first number is the Hartmann number: $Ha = B_0 a\sqrt{\frac{\sigma}{\rho\nu}}$ which is the ratio between electromagnetic forces and viscous forces. This number is of primary importance since in this inertialess study, the velocity field results from an equilibrium between these two forces. To characterize the alternating magnetic field, the shielding parameter $R_\omega = \mu\sigma\frac{\omega}{p}a^2$ is generally considered. This parameter quantifies the magnetic field skin depth with respect to the cylinder radius. For the third number, we have chosen the interaction parameter: $N = \frac{p\sigma{B_0}^2}{\rho\omega}$ where, as for the two previously formed numbers, only known quantities appear. In our study, the interaction parameter is assumed to be large in comparison with unity. The equations will be written in dimensionless form using the following characteristic scales:

- a for the distance.
- $\frac{\omega a}{p}$ for the velocity.
- $\frac{\omega a^2}{p}$ for the stream function ψ.
- $B_0 a$ for potential vector $\vec{A}$.
- $\frac{B_0}{\mu}$ for the surface current density j_0.

2.4. Stream function ψ and potential vector $\vec{A}$ formulation

As we study a two-dimensional problem, it is interesting to solve the curl of the momentum equation using the stream function ψ defined as $\vec{V} = \overrightarrow{\text{curl}}(\psi\vec{k})$. The pressure is therefore eliminated from the Navier Stokes equation (4). The magnetic field can also be formulated in terms of the potential vector $\vec{A}$ ($\vec{B} = \overrightarrow{\text{curl}}\vec{A}$) in which the axial component A_z is the only non zero component. The field $\vec{A}$ satisfies $\text{div}\vec{A} = 0$ and, as a consequence, the Coulomb gauge can be adopted. The problem is more easily analyzed in a frame of reference rotating with the magnetic field. In this frame, the magnetic field is steady but the cylinder rotates with an angular velocity: $-\frac{\omega}{p}\vec{k}$. As Moffatt (1978) pointed out, the Coriolis force arising from the change of frame is irrotational so it is compensated by a pressure adjustment and does not affect the velocity field. Neglecting inertial terms, the curl of the Navier Stokes equations (4) can be written in the coordinate system (r, Φ, z) where $\Phi = \theta - \frac{\omega}{p}t$:

$$\nu\Delta(\Delta(\psi)) = \frac{1}{\rho}\overrightarrow{\text{curl}}(\vec{j} \wedge \vec{B}) \cdot \vec{k} \tag{9}$$

with $\Delta = \frac{\partial^2}{\partial r^2} + \frac{1}{r}\frac{\partial}{\partial r} + \frac{1}{r^2}\frac{\partial^2}{\partial \Phi^2}$. Using the characteristic scales defined in the previous section, the following system can be obtained (the non-dimensional variables are noted with the exponent $*$):

$$\begin{aligned}\Delta^*(\Delta^*(\psi^*)) = \frac{Ha^2}{r^*}\Bigg[&\frac{\partial A_z^*}{\partial \Phi}\frac{\partial}{\partial r^*}\left(\frac{1}{r^*}\left(-\frac{\partial \psi^*}{\partial \Phi}\frac{\partial A_z^*}{\partial r^*} + \frac{\partial \psi^*}{\partial r^*}\frac{\partial A_z^*}{\partial \Phi}\right)\right)\\ &- \frac{\partial A_z^*}{\partial r^*}\frac{\partial}{\partial \Phi}\left(\frac{1}{r^*}\left(-\frac{\partial \psi^*}{\partial \Phi}\frac{\partial A_z^*}{\partial r^*} + \frac{\partial \psi^*}{\partial r^*}\frac{\partial A_z^*}{\partial \Phi}\right)\right)\Bigg].\end{aligned} \tag{10}$$

For the potential vector $\vec{A}$, the uncurl of equation (2) reduces to:

$$\Delta^*(A_z^*) = -\frac{R_\omega}{r^*}\left[\frac{\partial \psi^*}{\partial r^*}\frac{\partial A_z^*}{\partial \Phi} - \frac{\partial \psi^*}{\partial \Phi}\frac{\partial A_z^*}{\partial r^*}\right]. \tag{11}$$

The boundary conditions associated with set of equations are deduced from section (2.1) and written in the rotating frame:

$$\text{at } r^* = 1\text{: } \psi^* = 0,\ \frac{\partial \psi^*}{\partial r^*} = 1,\ \frac{\partial A_z^*}{\partial r^*} = \cos(p\Phi) \tag{12}$$

A_z^* is defined with respect to an arbitrary constant when the Coulomb gauge is imposed. We have imposed $A_z^* = 0$ at $r^* = 0$. Discussion of the physical mechanisms will be undertaken using quantities which have been calculated in the rotating field frame in order to allow a more precise description of quantities that would be time-dependent in the laboratory frame. Nevertheless, the evolution of the azimuthal velocity versus r will be plotted in the laboratory frame. For the sake of clarity, the $*$ exponent, which denotes non-dimensional variables, will be omitted.

2.5. Numerical method

We used routines taken from BIHAR and SLATEC libraries to solve the biharmonic equation for ψ and the Poisson equation for A_z respectively. Further details on the numerical method for solving theses equations can be found in Swarztrauber and Sweet (1973) and Bjorstad (1980). The domain is divided into a regular mesh of m grid points in the radial direction and n grid points in the azimuthal direction. The boundary conditions on the discrete contour and the source terms (right hand side of equation (10) and (11)) on the inner grid points both have to be specified. Each source term is discretized on the mesh using a finite difference technique on a nine-point stencil in order to obtain a second order accurate expression for the derivatives. The equation for A_z and the equation for ψ are solved with a guessed value (f_{old}) for the source term (zero for the first step) and the solution (f_{new}), after relaxation, is used as a guess for the next step. It is often necessary to under-relax the solution (sometimes less than 1%, that is to say f_{old} is replaced by $0.99\ f_{old} + 0.01\ f_{new}$) especially for high values of R_ω or Ha. We stopped the computation when the maximum of difference ($\|f_{old} - f_{new}\|$) between two successive iterations became small enough on each grid point (using double precision, we choose a difference of 10^{-14}). In the results presented below, we have used a $m \times n = 128 \times 64$ grid.

2.6. Validating the numerical method for $p = 1$

In order to check our numerical procedure, equations (10) to (12) have been solved in some particular cases for which the solution has already been obtained in previous papers.

Neglecting the induced magnetic field ($R_\omega = 0$ in equation (11)), we have compared our solution with the numerical results obtained by Hall and Walker (1993) for two values of the Hartmann number. As shown in figure 3 a,b, the shape of the velocity streamlines is very similar and the minimum value of ψ has been compared to that plotted in figure (2 a,b) in Hall and Walker (1993) and the difference remains smaller than approximately 10%. Furthermore, it is known from Hall and Walker (1993) that the flow is characterized by $\psi_{min} = -0.71 \cdot Ha^{-2/3}$ for high values of the Hartmann number. For a 128×64 grid, it is surprising that the difference with this asymptotic law is already less than 2 to 3% for $Ha = 10$. Using the same grid, this difference does not exceed 4% for $Ha = 200$ and can be reduced to 2.6% with a 256×256 grid. This first test confirms the efficiency of the technique which has been adopted for solving the biharmonic equation (10).

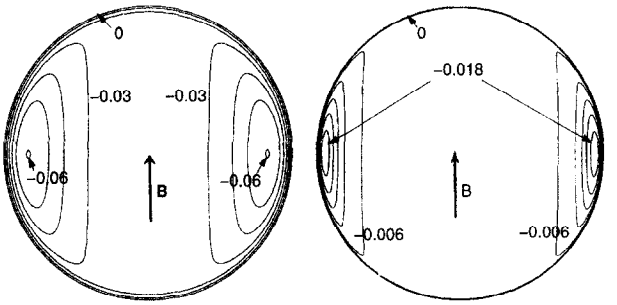

a) $\psi = -0.01k$ with $k = [0, 6]$. b) $\psi = -0.003k$ with $k = [0, 6]$.

Fig. 3. – Velocity streamlines for $R_\omega = 0$. a) $Ha = 40$; b) $Ha = 200$.

For different values of the shielding parameter R_ω, figure 4 shows that our solution agrees quite satisfactorily with the velocity field equation (13) obtained by Dahlberg (1972). We can, henceforth, note that $\frac{v}{Ha^2}$ is only dependent upon R_ω and r. In the cases we have tested, this series expansion was found to converge very rapidly

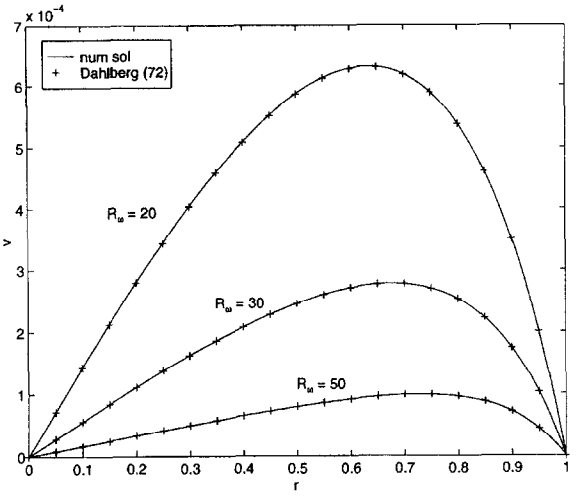

Fig. 4. – Azimuthal velocity versus r for $Ha = 1$ and $R_\omega = 20, 30, 50$.

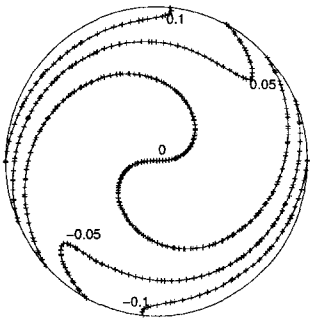

Fig. 5. – Magnetic field lines for $Ha = 1$ and $R_\omega = 50$; – : numerical solution + : analytical solution.

and only the first five terms have been retained.

$$v = \frac{Ha^2}{16}\frac{1}{|D|^2} r \sum_{n=0}^{+\infty} \frac{\left(1 - r^{4n+2}\right)\left(\frac{1}{4}R_\omega\right)^{2n}}{(2n+1)(2n+1)!((n+1)!)^2} \tag{13}$$

where $D = \mathcal{J}_0\left(\sqrt{iR_\omega}\right) - \mathcal{J}_2\left(\sqrt{iR_\omega}\right)$ and where $\mathcal{J}_\beta(x)$ is the Bessel function of the first kind. Figure 5 shows the magnetic field lines which match their analytical expression $A_z = \Re\left(\frac{-2\mathcal{J}_1\left(\sqrt{iR_\omega}r\right)}{\sqrt{iR_\omega}D} \cdot e^{i\Phi}\right)$ perfectly.

This second test confirms the validity of the resolution of the Poisson equation (11) and the correct description of the right-hand side source term of equation (10)).

3. Results

3.1. Influence of Ha and R_ω on the azimuthal flow when $p = 1$

In order to study the influence of the two dimensionless parameters R_ω and Ha, the evolution of $\frac{v_{max}}{Ha^2}$ versus R_ω has been plotted in figure 6 for different Hartmann numbers (v_{max} is the maximum value of the azimuthal velocity on $(r, \theta) \in [0, 1] \times [0, 2\pi]$).

When $R_\omega \ll 1$, (a restriction which can be extended, in practice, to $R_\omega < 1$), and for all Ha, v_{max} is independent of R_ω. This confirms that, in the low frequency limit, the shielding parameter is not relevant, due

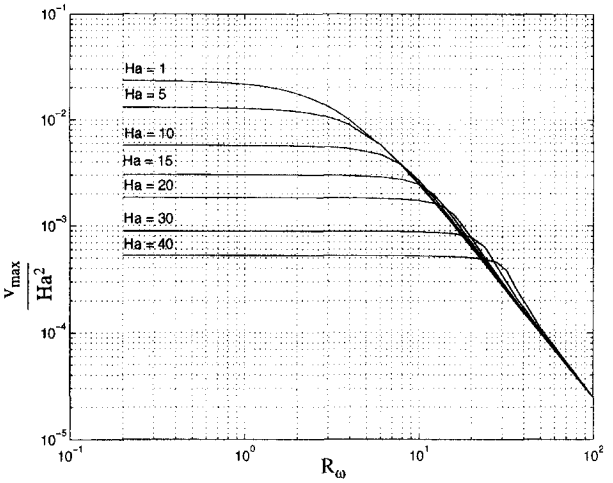

Fig. 6. – Evolution of $\frac{v_{max}}{Ha^2}$ versus R_ω for $Ha = 1, 5, 10, 15, 20, 30$ and 40.

to the fact that the skin depth would be larger than the cylinder radius, which would make no sense. Figure 6 also shows that, when $Ha \gg 1$, the fluid is close to synchronism, this means that the maximum velocity in the azimuthal direction is of order of unity: $v_{max} \simeq O(1)$.

When $R_\omega > 1$, the magnetic field imposed by the current sheet is expelled from the core flow by the induced currents. The driving azimuthal force is therefore weakened and the maximum velocity diminishes. According to the value of Ha, two different types of behaviour can be distinguished:

• For $Ha < 1$, the flow velocity is negligible when compared to that of the magnetic field, whatever the value of R_ω. The rigid body approximation is therefore valid and v_{max} can be deduced from equation (13). The limit case $Ha = 1$ has been plotted in figure 6. When $R_\omega \gg 1$ the linear decrease of v_{max} is such that $\frac{v_{max}}{Ha^2} \approx {R_\omega}^{-2}$ and is in agreement with Moffatt's (1965) asymptotic analysis. The physical explanation of this asymptotic evolution is quite simple and will be presented in section (4.3) for any value of the number of poles.

• For $Ha > 1$, the fluid rotates at synchronous velocity as long as $R_\omega < \frac{Ha}{\sqrt{2}}$ and, thus far, none of the previous papers have envisaged this situation. Although not visible in figure 6, a slight decrease of the velocity exists when R_ω increases, as discussed earlier. As soon as $R_\omega > \frac{Ha}{\sqrt{2}}$, the fluid velocity is no longer synchronous and the rigid body approximation is valid again. As a consequence, all the curves match with the curve obtained for $Ha = 1$.

3.2. Detailed structure of the flow and magnetic field

In this section, we have chosen the particular value $Ha = 30$ to illustrate the behavior of the flow and the magnetic field.

In figure 7, the radial profiles of the mean, maximum and minimum azimuthal velocity for $\Phi \in [0, 2\pi]$ are plotted for different values of R_ω. As long as $R_\omega < \frac{Ha}{\sqrt{2}}$, the fluid rotates slightly faster than the magnetic field with the exception of the fluid in the Hartmann layer near $r = 1$. This hyper-synchronism can be explained by the lack of symmetry of the Hartmann layer which causes a secondary recirculating flow in the core. This has been described in Alemany and Moreau (1977). When R_ω increases, the fluid no longer rotates at synchronism and the rigid body approximation again becomes valid. The flow is then purely azimuthal and the velocity field is described by equation (13).

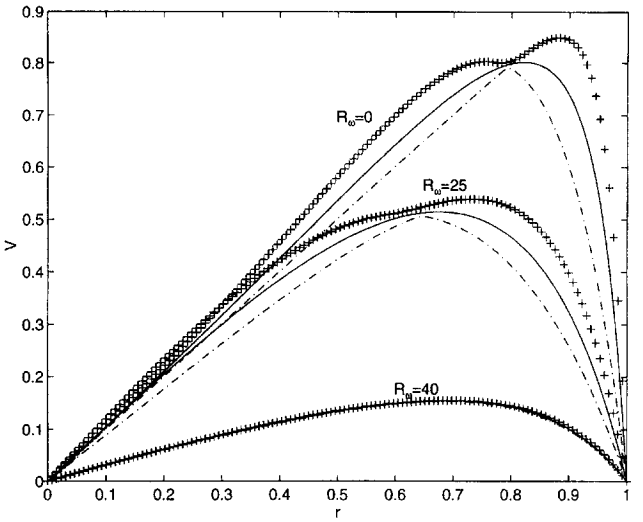

Fig. 7. – Azimuthal velocity v versus r for $Ha = 30$ and $R_\omega = 0$, 25 and 40. azimuthal maximum (+), minimum (−·), mean (−) of azimuthal velocity.

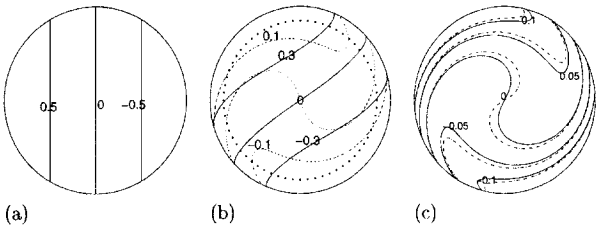

Fig. 8. – Magnetic field lines for $Ha = 30$; a) $R_\omega = 0$, b) $R_\omega = 19$ and c) $R_\omega = 40$: the solid lines represents the solution taking into account the velocity field; the dashdot lines represent the solution for the rigid body approximation.

The magnetic field lines are shown in figure (8 a,b,c) for various R_ω. When $R_\omega = 0$ (figure (8 a)), the magnetic field enters the fluid perfectly and is not affected by the presence of the metal. In figure (8 c) the rigid body approximation begins to be valid: here the difference between the magnetic field and the flow velocity is high enough to neglect the fluid velocity in the magnetic field calculation. In figure (8 b), two distinct zones appear and have been separated by a dotted circle:

- a thin layer near the wall where the field is convected by the fluid.
- a core region where the magnetic field only diffuses due to the fact that the fluid is at synchronism, which eliminates any source terms in the induction equation.

In this figure, it is worth noting the considerable difference between the real magnetic field solution and that which would be obtained by neglecting the effect of the fluid velocity in the induction equation.

Plotting the stream function reveals the velocity field. The case $Ha = 30$ has been treated in figure (9 a,b,c). For R_ω varying from 0 to $\frac{Ha}{\sqrt{2}}$, the velocity field in the core is aligned with the magnetic field, both being shifted with respect to their direction when $R_\omega = 0$. For $R_\omega > \frac{Ha}{\sqrt{2}}$, the recirculating flow in the core weakens and then disappears.

This rapid transition to an axisymmetric regime is illustrated in figure 10 which displays the evolution with respect to R_ω of the ratio between the recirculating flow rate and the total flow rate of one eddy, in the

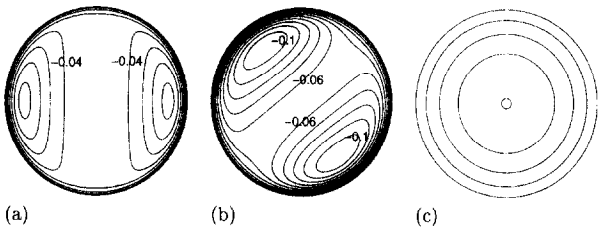

Fig. 9. – Streamlines for $Ha = 30$; a) $R_\omega = 0$, $\psi = -0.01k$ with $k = [0, 7]$, b) $R_\omega = 19$, $\psi = -0.01k$ with $k = [0, 10]$, and c) $R_\omega = 40$, $\psi = -0.1k$ with $k = [0, 4]$.

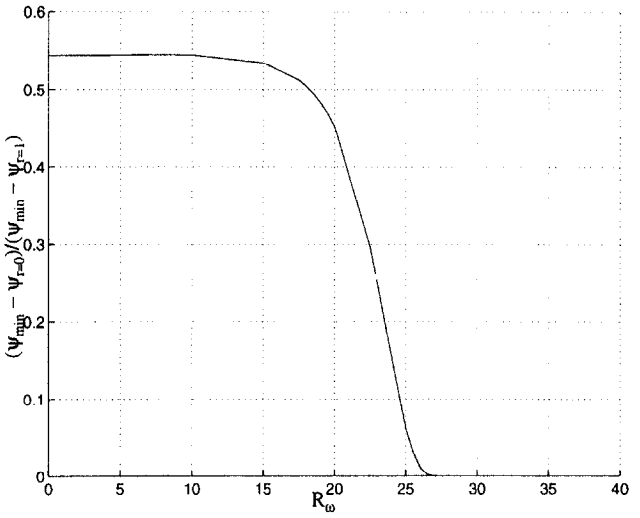

Fig. 10. – Ratio between the recirculating flow rate of one eddy to the total flow rate versus R_ω for $Ha = 30$.

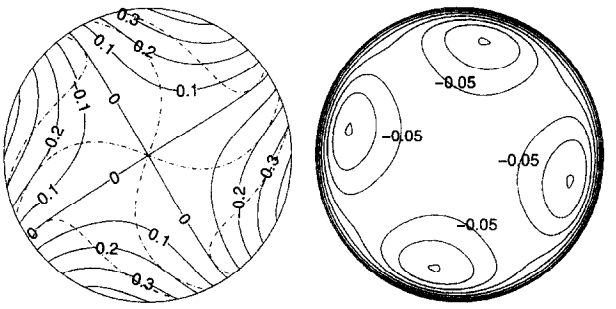

a) – $A_z = 0.1k$ and $k = [-4, 4]$. $-\cdot-$ $A_z = 0.1k$ and $k = [-1, 1]$.

b) $\psi = -0.01k$ and $k = [0, 7]$.

Fig. 11. – Magnetic field lines and velocity streamlines for $p = 2$, $Ha = 30$ and $R_\omega = 10$ (solid lines display the solution when the velocity field is taken into account whereas the dashdot lines are the solution when the rigid body approximation is used).

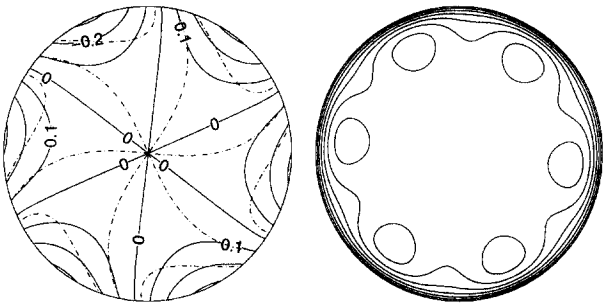

a) $-$ $A_z = 0.1k$ and $k = [-3, 3]$.
$-\cdot-$ $A_z = 0.1k$ and $k = [-1, 1]$.

b) $\psi = -0.01k$ and $k = [0, 6]$.

Fig. 12. – Same legend as figure 11 for $p = 3$, $Ha = 30$ and $R_\omega = 7$.

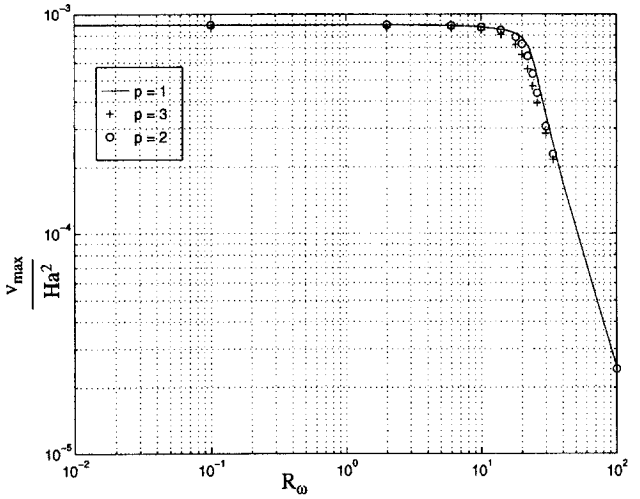

Fig. 13. – Evolution of $\frac{v_{max}}{Ha^2}$ versus R_ω for $Ha = 30$ and $p = 1, 2, 3$.

magnetic field frame:

$$\frac{\psi_{min} - \psi_{r=0}}{\psi_{min} - \psi_{r=1}}. \tag{14}$$

3.3. Influence of magnetic field polarity

For $Ha = 30$ and $R_\omega = 10$, figure 11 shows the magnetic field and velocity patterns for $p = 2$. The presence of $2p$ recirculating cells can be observed, as mentioned by Alemany and Moreau (1977). Increasing the number of poles results in the confinement of the magnetic field to the proximity of the wall, which, in turn, weakens the electromagnetic forces in the core. This is confirmed in figure 12 plotted for $2p = 6$, and the recirculating cells are observed closer to the wall. Finally, figure 13 shows that changing the number of poles does not affect the evolution of $\frac{v_{max}}{Ha^2}$ with respect to R_ω.

4. Discussion

The above descriptive approach does not facilitate understanding of the prevailing physical mechanisms. In section (4.1), a simplified model for velocity and magnetic fields is proposed to build an order of magnitude

analysis and to give an explanation for the transition from the synchronous regime $v_{max} \approx 1$ to the rigid body regime where $\frac{v_{max}}{Ha^2} \approx R_\omega^{-2}$. Finally, a simple analysis of the regime $R_\omega \gg 1$ will be proposed.

4.1. The ring model

It has been observed that the velocity field is only slightly affected by an increase of R_ω as long as $R_\omega < \frac{Ha}{\sqrt{2}}$ and $Ha \gg 1$. For low values of R_ω, we shall establish the exact expression of the velocity in order to build a simplified flow model. In the laboratory frame, a space and time averaging of the forces results in the flow having only an azimuthal component. Its equation is:

$$\frac{\partial^2 v}{\partial r^2} + \frac{1}{r}\frac{\partial v}{\partial r} - \frac{v}{r^2}\left(1 + \frac{Ha^2}{2} r^{2p}\right) = -\frac{Ha^2}{2} r^{2p-1} \tag{15}$$

with the following boundary conditions:

$$v(0) = 0 \text{ and } v(1) = 0. \tag{16}$$

This Bessel equation has the following solution:

$$v(r) = \left(r - \frac{\mathcal{I}_{\frac{1}{p}}\left(\frac{Ha}{p\sqrt{2}} r^p\right)}{\mathcal{I}_{\frac{1}{p}}\left(\frac{Ha}{p\sqrt{2}}\right)} \right) \tag{17}$$

where $\mathcal{I}_\beta(x)$ is the modified Bessel function of the first kind. When $Ha \gg 1$ this solution can be approximated by:

$$v \approx r - \frac{e^{\frac{Ha}{p\sqrt{2}}(r^p - 1)}}{r^{\frac{p}{2}}} \approx r - e^{\frac{Ha}{p\sqrt{2}}(r^p - 1)} \tag{18}$$

and has a maximum value for $r_s = 1 - \frac{\sqrt{2}}{Ha} \ln\left(\frac{Ha}{\sqrt{2}}\right)$. Let us approximate the velocity difference between the fluid and the magnetic field by the following function:

$$\begin{cases} 0 \text{ if } 0 < r < r_s \\ \bar{\omega} = \dfrac{1}{1 - r_s} \displaystyle\int_{r_s}^{1} \left(1 - \frac{v}{r}\right) dr \approx \left[\ln\left(\frac{Ha}{\sqrt{2}}\right)\right]^{-1} \text{ if } r_s < r < 1. \end{cases} \tag{19}$$

This approximation is equivalent to considering a rigid hollow cylinder (or one with an insulating core) with a relative angular velocity equal to $\bar{\omega}$. A scheme of the model is represented in figure 14. The calculation is made easier by introducing the complex notation for the vector potential which can be written: $A_z(r, \theta, t) = \Re(A(r) \cdot e^{i(p\theta - \omega t)})$. Neglecting the curvature in the ring domain where $r_s < r < 1$ (for example, $r_s = 0.85$ when $Ha = 30$) the vector potential equation can be written:

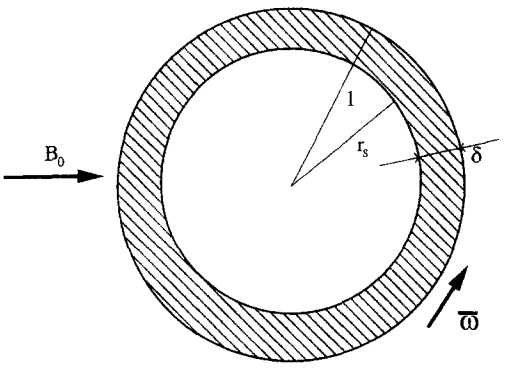

Fig. 14. – Equivalent ring model.

for $r_s < r < 1$:

$$\frac{\partial^2 A}{\partial r^2} - \alpha^2 A = 0 \tag{20}$$

which has the solution:

$$A = C_1 \cdot \mathrm{e}^{\alpha r} + C_2 \cdot \mathrm{e}^{-\alpha r} \quad \text{where } \alpha = \sqrt{-ipR_\omega \bar{\omega}} \tag{21}$$

for $0 < r < r_s$:

$$\frac{\partial^2 A}{\partial r^2} + \frac{1}{r}\frac{\partial A}{\partial r} - \frac{p^2}{r^2} A = 0 \tag{22}$$

which has the solution:

$$A = C_3 \cdot r^p + \frac{C_4}{r^p} \tag{23}$$

The following boundary conditions allow the determination of the four coefficients C_1, C_2, C_3 and C_4:

- when $r = 1$, $\frac{\partial A}{\partial r} = -1$
- when $r = r_s$, $[A] = 0$ and $[\frac{\partial A}{\partial r}] = 0$
- when $r = 0$, $A = 0$ is imposed

The solution of the set of linear equation gives:

$$C_1 = \frac{p}{\alpha \cdot C}\left(r_s + \frac{p}{\alpha}\right) r_s^{2(p-1)} \mathrm{e}^{-\alpha r_s} \tag{24}$$

$$C_2 = \frac{p}{\alpha \cdot C}\left(r_s - \frac{p}{\alpha}\right) r_s^{2(p-1)} \mathrm{e}^{\alpha r_s} \tag{25}$$

$$C_3 = \frac{2p\, r_s^{p-1}}{\alpha \cdot C} \tag{26}$$

$$C_4 = 0 \tag{27}$$

$$\text{where } C = -r_s^{p-1}\left(\left(\frac{p}{\alpha} + r_s\right)\mathrm{e}^{\alpha(1-r_s)} + \left(\frac{p}{\alpha} - r_s\right)\mathrm{e}^{-\alpha(1-r_s)}\right)$$

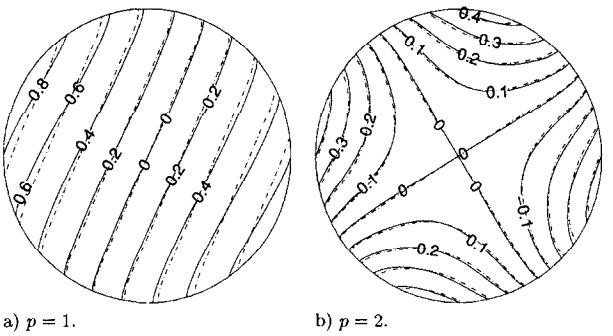

a) $p = 1$. b) $p = 2$.

Fig. 15. – Magnetic field distribution for $R_\omega = 10$ and $Ha = 30$: the solid lines represent the exact numerical solution; dashdot lines represent the solution obtained with the ring model.

Figures (15 a,b) show the good agreement between the magnetic field lines obtained in solving the set of equations (10) to (12) and those obtained with the above ring model. These results show that the magnetic boundary layer at the wall is controlled by the Hartmann layer. Finally it can be noted that the flow created by the magnetic field later determines the behavior of the magnetic field.

4.2. Justifying the transition criterion

In the next two sections, dimensional variables will be used.

The results of the previous section demonstrate that the orders of magnitude introduced in the ring model are pertinent. To explain the transition occurring at $R_\omega = \frac{Ha}{\sqrt{2}}$, let us detail the characteristic time scales which should be used to build a meaningful shielding parameter R_ω. Usually, the shielding parameter is formed as the ratio of two characteristic times, namely the diffusive time, t_d and the convective time, t_c of the magnetic field, constructed with the magnetic diffusivity $\frac{1}{\mu\sigma}$, the radius of the cylinder a and the magnetic field velocity $\frac{\omega}{p}a$.

$$t_d = \frac{a^2}{\frac{1}{\mu\sigma}} \quad \text{and} \quad t_c = \frac{a}{\frac{\omega}{p}a} \tag{28}$$

$$\frac{t_d}{t_c} = R_\omega \tag{29}$$

These characteristic time scales are only meaningful when the rigid body approximation is valid because, when so, the whole cylinder contributes to the expulsion of the magnetic field from the core. On the contrary, when the Hartmann number is high enough to drive the core flow at synchronism, only the wall layer has a distortion effect on the magnetic field. As long as this distortion effect is moderate, the radial component of the magnetic field fully interacts with the axial electric currents, thus giving rise to a driving azimuthal force. For a given Hartmann number, increasing $\frac{\omega}{p}$ also increases the relative velocity between the magnetic field and the fluid. The resulting convective mechanism weakens the radial component of $\vec{B}$ and reinforces the azimuthal component thereby diminishing the intensity of the rotating forces in the fluid. Therefore, for an infinitely high value of $\frac{\omega}{p}$, the almost complete disappearance of the radial component is in agreement with the evolution in R_ω^{-2} which will be discussed in section (4.3). For a given Ha, the transition observed in figure 6 will occur when the characteristic length along which the magnetic field has been swept in the azimuthal direction is of the same order of magnitude, δ, as the thickness of the hydrodynamic boundary layer through which the field penetrates by a diffusion mechanism. The knowledge of the thickness $\delta \simeq \frac{\sqrt{2}}{Ha}\ln(\frac{Ha}{\sqrt{2}})a$ and of the mean azimuthal velocity $\bar{\omega} = \left[\ln(\frac{Ha}{\sqrt{2}})\right]^{-1}\frac{\omega}{p}a$ allows the following characteristic time scales to be constructed:

$$t_d = \frac{\delta^2}{\frac{1}{\mu\sigma}} \quad \text{and} \quad t_c = \frac{\delta}{\left[\ln(\frac{Ha}{\sqrt{2}})\right]^{-1}\frac{\omega}{p}a} \tag{30}$$

Equating these two times gives the transition criterion:

$$R_\omega = \frac{Ha}{\sqrt{2}}. \tag{31}$$

4.3. THE ASYMPTOTIC REGIME: $R_\omega \gg \frac{Ha}{\sqrt{2}}$

For high values of R_ω the magnetic field is confined in a skin layer of thickness $\delta_e = {R_\omega}^{-1/2} a$. The order of magnitude of the azimuthal component B_θ is deduced from (8):

$$B_\theta \simeq B_0.$$

The radial component is deduced from the magnetic flux conservation:

$$B_r \simeq \frac{\delta_e}{a} p B_0.$$

An approximate value of the axial electric current density can be obtained from the Ampere theorem $\overrightarrow{\text{curl}\vec{B}} = \mu\vec{j}$:

$$j_z \simeq \frac{1}{\mu}\left\{\frac{B_0}{\delta_e} - \frac{1}{a} B_0 \frac{\delta_e}{a} p\right\} \simeq \frac{1}{\mu}\left\{\frac{B_0}{\delta_e}\right\}.$$

For high values of R_ω, the thickness of the hydrodynamic boundary layer is equal to that of the electromagnetic skin depth, δ_e. Then the azimuthal balance between electromagnetic and viscous forces can be written:

$$\rho\nu \frac{v}{\delta_e^2} \simeq \left(\frac{1}{\mu}\frac{B_0}{\delta_e}\right) \cdot \left(p B_0 \frac{\delta_e}{a}\right)$$

which gives the result:

$$\frac{v}{\frac{\omega}{p} a} = \frac{Ha^2}{R_\omega^2}.$$

4.4. A REMARK ABOUT THE UNIQUENESS OF THE FLOW IN THE ASYMPTOTIC REGIME

The method above described gives only one steady state solution. Nevertheless, as pointed out by Moffatt (1978), two different steady state solutions can be reached depending on the initial conditions. When the magnetic field is suddenly switched on with a fluid and a wall both at rest, this leads to the solution which has been described in this paper ($v_{core} \sim \Omega_1\ r$). On the contrary, according to Moffatt, starting with a fluid and a wall both rotating at synchronism and suddenly stopping the wall rotation should make the core velocity rotate with an angular velocity only slightly smaller than that of the magnetic field ($v_{core} \sim \Omega_2\ r$).

An unsteady version of the numerical technique described above has been developed with the aim of finding this second steady state solution Ω_2 for the core velocity. Starting from synchronism at $t = 0$, the time evolution of the flow has shown an oscillatory behavior. It has first decreased to a low value close to Ω_1, then has suddenly increased to a value close to Ω_2 but has finally converged towards the solution Ω_1 having the highest slip velocity.

An inefficient precision of the time scheme could be inferred in addition to a lack of stability of the solution Ω_2. Nevertheless the unsteady behavior of this problem appears very rich and could be the matter of a further study, but this is beyond the scope of the present paper.

5. Conclusion

A numerical and analytical study of the flow driven by a rotating field in a cylindrical cavity was performed for any value of the Hartmann number, Ha, and of the shielding parameter, R_ω. For high values of the Hartmann number the flow can have two different patterns depending upon the value of R_ω:

• for $R_\omega < \frac{Ha}{\sqrt{2}}$, the flow consists of a Hartmann layer at the wall and of a core region with recirculating eddies which cause an azimuthal velocity slightly greater than that of the magnetic field. It has been noted that the number of these recirculating eddies is equal to the number of poles. When crossing the Hartmann layer, the magnetic field is subjected to a convection mechanism, which has the effect of shifting the magnetic field lines in the core where they have a constant direction and are governed only by a pure diffusion law. When R_ω increases from 0 to $\frac{Ha}{\sqrt{2}}$, the streamlines of the recirculating cells remain aligned with the magnetic field in the core.

• for $R_\omega > \frac{Ha}{\sqrt{2}}$, the flow still has a wall boundary layer and a core zone in which angular velocity follows a $\frac{Ha^2}{R_\omega^2}$ law. The intensity of the recirculating cells is so greatly reduced that the streamlines are almost circular. The magnetic field in the core is subjected to a strong distortion due to the effect of the considerable difference between its velocity and that of the fluid.

A simple equivalent model of the flow has been proposed. Reviewing the pertinent characteristic time and length scales made it possible to justify the transition observed when $R_\omega = \frac{Ha}{\sqrt{2}}$.

To get closer to a real situation, an improvement would certainly consist in taking into account inertial effects. If the condition $N \gg 1$ is not satisfied it is clear that certain regions of the plane parameters Ha and R_ω would be unstable as a function of Ha, R_ω and N. As indicated by Richardson (1974), the circulation is a decreasing function of the radius near the cylinder boundary, and the flow is therefore prone to instabilities of Taylor vortex type.

Acknowledgment. – The authors are indebted to Professor H.K. Moffatt for valuable remarks about the uniqueness of the solution.

REFERENCES

ALEMANY A., MOREAU R., 1977, Ecoulement d'un fluide conducteur de l'électricité en présence d'un champ magnétique tournant, *J. de Meca. Th. et Appl.*, **16**, 625-646.

BJORSTAD P. E., 1980, *Numerical solution of the biharmonic equation*, PhD thesis, Stanford.

DAHLBERG E., 1972, On the action of a rotating magnetic field on a conducting liquid. Technical Report AE-447, Aktiebolaget Atomenergi, Studsvik, Sweden.

DAVIDSON P. A., HUNT J. C. R., 1987, Swirling recirculating flow in a liquid-metal column generated by a rotating magnetic field, *J. Fluid Mech.*, **185**, 67-106.

DURAND E., 1968, *Magnétostatique*, Masson & Cie.

GELFGAT Y. M., PRIEDE J., 1995, MHD flows in a rotating magnetic field (a review), *Magnetohydrodynamics*, **31**, 188-200.

GELFGAT Y. M., PRIEDE J., SORKIN M. Z., 1991, Numerical simulation of mhd flow induced by magnetic field in cylindrical container of finite length. In *Proceedings on the Second International Conference on Energy Transfer in Magnetohydrodynamic flows*, Cadarache, 181-186.

HALL M. C., WALKER J. S., 1993, Heat and mass transfer through a liquid metal in an infinitely long, rotating cylinder with a uniform, transverse magnetic field, *Int. J. Heat & Mass Transf.*, **36**, 3509-3514.

MOFFATT H. K., 1965, On fluid flow induced by a rotating magnetic field, *J. Fluid Mech.*, **22**, 521-528.

MOFFATT H. K., 1978, Rotation of a liquid metal under the action of a rotating magnetic field. In *Proceedings of the Second Bat-Sheva International Seminar*, Beersheva, 45-62.

RICHARDSON A. T., 1974, On the stability of a magnetically driven rotating fluid flow, *J. Fluid Mech.*, **63**, 593-605.

SWARZTRAUBER P. N., SWEET R., 1973, The direct solution of the discrete poisson equation on a disk, *SIAM J. Num. Anal.*, **10**, 900-907.

(Manuscript received March 04, 1997;
revised September 23, 1997;
accepted October 07, 1997.)